Journal for ImmunoTherapy of Cancer

Localized ablative immunotherapy drives de novo CD8$^+$ T-cell responses to poorly immunogenic tumors

Ashley R Hoover ,[1] Saghar Kaabinejadian ,[2] Jason R Krawic ,[2] Xiao-Hong Sun,[3] Abdul Rafeh Naqash,[4] Qian Yin,[5] Xinbo Yang,[6] K Christopher Garcia,[6] Mark M Davis,[7] William H Hildebrand,[2] Wei R Chen [1]

To cite: Hoover AR, Kaabinejadian S, Krawic JR, *et al*. Localized ablative immunotherapy drives de novo CD8$^+$ T-cell responses to poorly immunogenic tumors. *Journal for ImmunoTherapy of Cancer* 2022;**10**:e004973. doi:10.1136/jitc-2022-004973

► Additional supplemental material is published online only. To view, please visit the journal online (http://dx.doi.org/10.1136/jitc-2022-004973).

Accepted 17 September 2022

For numbered affiliations see end of article.

Correspondence to
Dr Wei R Chen;
wei-r-chen@ou.edu

ABSTRACT

Background Localized ablative immunotherapies hold great promise in stimulating antitumor immunity to treat metastatic and poorly immunogenic tumors. Tumor ablation is well known to release tumor antigens and danger-associated molecular patterns to stimulate T-cell immunity, but its immune stimulating effect is limited, particularly against metastatic tumors.

Methods In this study, we combined photothermal therapy with a potent immune stimulant, N-dihydrogalactochitosan, to create a local ablative immunotherapy which we refer to as laser immunotherapy (LIT). Mice bearing B16-F10 tumors were treated with LIT when the tumors reached 0.5 cm^3 and were monitored for survival, T-cell activation, and the ability to resist tumor rechallenge.

Results We found that LIT stimulated a stronger and more consistent antitumor T-cell response to the immunologically 'cold' B16-F10 melanoma tumors and conferred a long-term antitumor memory on tumor rechallenge. Furthermore, we discovered that LIT generated de novo CD8$^+$ T-cell responses that strongly correlated with animal survival and tumor rejection.

Conclusion In summary, our findings demonstrate that LIT enhances the activation of T cells and drives de novo antitumor T-cell responses. The data presented herein suggests that localized ablative immunotherapies have great potential to synergize with immune checkpoint therapies to enhance its efficacy, resulting in improved antitumor immunity.

WHAT IS ALREADY KNOWN ON THIS TOPIC

⇒ Combining localized tumor ablation with intratumoral administration of a potent immunostimulant drives strong antitumor immunity against poorly immunogenic tumors. Not only does this combination cure the treated tumor and eradicate untreated metastases, but it confers long-term protection against tumor rechallenge.

WHAT THIS STUDY ADDS

⇒ This study demonstrates that this novel localized ablative immunotherapy drives de novo T-cell responses as a unique immunological mechanism in inducing the antitumor immunity.

HOW THIS STUDY MIGHT AFFECT RESEARCH, PRACTICE OR POLICY

⇒ This study shows that this novel therapy has great potential to synergize with immune checkpoint therapies and other immunotherapies, hence providing new strategies to improve the efficacy in treating metastatic cancers.

BACKGROUND

Poorly immunogenic tumors are difficult targets for current immunotherapeutic strategies, as they rely on the existing antitumor immune responses to be effective. There are several methods or mechanisms by which tumor cells and/or the tumor immune microenvironment (TIME) contribute to immune escape, thus reducing immune infiltration and tumor killing. One such method is reducing the expression of major histocompatibility complex (MHC) class I molecules on the tumor surface, thus preventing adequate CD8$^+$ T-cell priming.[1–4] Another method is establishing an immunosuppressive environment with the help of T regulatory cells[5 6] or myeloid-derived suppressor cells.[7 8] We have developed a localized photo-ablative technique that combines local photothermal therapy (PTT) and intratumoral administration of an immune stimulant, N-dihydrogalactochitosan (GC). We refer to this therapy as laser immunotherapy (LIT). Previous work using the MMTV-PyMT mouse breast tumor model revealed that LIT globally modified the tumor microenvironment (TME) by initiating a type I/II interferon (IFN) cytokine signature.[9 10] Type I/II IFNs are critical for the generation of antitumor T-cell responses and play a crucial role in dendritic cell cross-presentation to T cells.[11–13] Single-cell RNA-sequencing of the tumor-infiltrating adaptive immune cells in the MMTV-PyMT tumor model revealed that B cells and both CD4$^+$ and CD8$^+$ T cells were highly activated following

LIT.[9 14] These results suggest that LIT can overcome some of these immune escape mechanisms, allowing the adaptive immune response to eliminate the tumors.

We hypothesize that the effect of LIT treatment is comprised of three consecutive phases. During the first phase, PTT disrupts the local TIME via direct tumor killing. The thermo-ablation induces immunogenic cell death (ICD), releasing danger-associated molecular patterns (DAMPs) and a variety of tumor antigens. The second phase involves ICD-induced recruitment of immune cells into the TIME. During the third phase, the addition of a strong immune stimulant, which drives a type I IFN response, allows for establishing an immunologically active TIME, potentiating an antitumor response. However, the underlying mechanism behind LIT's effects on T cells is still not clear. LIT could enhance the existing antitumor T-cell responses through the release of tumor antigens, and the addition of immune stimulation by GC could enable these cells to infiltrate the TME following LIT to initiate antitumor activity. Alternatively, LIT could also generate de novo T-cell responses through the release of tumor antigens, followed by potent immune stimulation, which can effectively eliminate the existing tumor and establish long-term antitumor immunity.

To uncover the mechanism of LIT, we used the B16-F10 melanoma tumor model. This tumor is characterized by very little immune cell infiltration, making it notoriously difficult to treat.[15] Our current study revealed that LIT successfully treated B16-F10 tumors and conferred long-term protection against tumor rechallenge. Analysis of the tumor-draining lymph nodes and the spleen revealed that CD28, CD25, and CD69 were upregulated on the surface of $CD8^+$ and $CD4^+$ T cells following LIT and PTT, all of which correlated with T-cell activation and antigen recognition. By identifying B16-F10 tumor specific peptides and screening them for T-cell activation, we found six peptides that generated T-cell responses following LIT. Interestingly, these same peptides also showed increased T-cell reactivity in the LIT-cured animals that rejected tumor rechallenge. Our results herein provide evidence that LIT generates de novo $CD8^+$ T-cell responses that correlate with long-term antitumor immunity.

MATERIALS AND METHODS

Cell line and antibodies

B16-F10 mouse melanoma cell line was obtained from American Type Culture Collection (ATCC). The cells were grown in DMEM F12K (Wisent), supplemented with 10% fetal bovine serum (Serum Source International) and maintained at 37°C in a 5% CO_2 humidified incubator. B16-F10 cells were implanted subcutaneously in C57BL/6 mice and tumors were harvested.

The anti-Kb monoclonal antibody (clone AF6-88.5.5.3) was purchased from BioXcell. Anti-Db (28-14-8S, ATCC) hybridoma was grown in serum-free media and purified in-house using Protein G Sepharose column (GE Healthcare, Sweden). The monoclonal antibodies (clones 28-14-8 (anti-Db) and AF6-88.5.5.3 (anti-Kb)) were used to isolate the MHC class I alleles (Db and Kb) and purify the Db-associated and Kb-associated peptides from the tumors as well as staining of the B16-F10 cells to determine cell surface expression of Db and Kb using flow cytometry.

Flow cytometry

To determine the expression of the MHC class I molecules (Db and Kb) on the surface of B16-F10 cells, they were seeded at 5×10^5 cells/well in 6-well plates in complete growth medium. The cells were treated with 50 U/mL recombinant mouse IFN-γ for 12, 24 and 48 hours after which the surface expression of Db and Kb was determined by flow cytometry. Clone 28-14-8 and AF6-88.5.5.3 monoclonal antibodies were used for Db and Kb staining, respectively.

The cells were stained with 1 µg of anti-Kb and anti-Db monoclonal antibodies for 30 min followed by PE-conjugated goat anti-mouse IgG for 30 min. Cells were analyzed on a FACSCalibur instrument (BD Biosciences) and the data analysis was performed using FlowJo Software (Tree Star, Ashland, Oregon, USA).

Splenocytes were stained for flow cytometry. Antibodies used for spleen staining include: CD3 (AF700, BioLegend), CD4 (PE/Dazzle, BioLegend), CD8 (FITC, Tonbo Bioscience), CD25 (BV-785, BioLegend), CD28 (APC, Tonbo Bioscience), CD44 (PerCP-Cy5.5, Tonbo Bioscience), CD62L (APC-Cy7, Tonbo Bioscience), CD69 (BV605, BioLegend), and Foxp3 (PE, BioLegend). Cells were also stained with the ghost violet 510 viability dye (Tonbo Bioscience). Briefly, 5×10^6 cells were stained for 20 min on ice with viability dye and cell surface CD antibodies. Cells were then washed with 1× phosphate-buffered saline (PBS) and fixed and permeabilized using the Foxp3 intracellular staining kit (eBioscience) according to manufacturer's instructions. Cells were analyzed using the LSR II (BD Biosciences). Data was evaluated using FlowJo V.10.7 and graphed using GraphPad Prism. Mean fluorescent intensity (MFI) values were generated via Flow Jo. Values were normalized to the untreated which was set to the value of 1 to calculate the fold change. One-way analysis of variance (ANOVA) was used for statistical analysis of the mean expression data. P values = *0.5, **0.05, **0.005, ****0.0005.

Isolation of MHC class I Db and Kb molecules and peptide identification

To identify the H2-Db and H2-Kb associated peptides from the tumors, traditional affinity chromatography was employed using the above-mentioned anti H2-Kb and anti H2-Db monoclonal antibodies. Immunoaffinity columns were generated by coupling 2 mg of the purified antibodies to 1 mL of Matrix (CNBr-activated Sepharose 4 Fast Flow). Two rounds of purification were performed on 4.5 g and 4.09 g of tumor with affinity columns set up in series so that both H2-Db and H2-Kb MHC/peptide complexes of each tumor were isolated and purified.

MHC/peptide complexes were extracted from B16-F10 tumors as previously described. Briefly, the tumors were flash frozen in liquid nitrogen, pulverized under cryogenic conditions using mixer mill (MM400, RETSCH) and resuspended in lysis buffer comprised of Tris pH 8.0 (50 mM), IGEPAL, 0.5%, NaCl (150 mM) and complete protease inhibitor cocktail (Roche, Mannheim, Germany). After incubation for 1 hour at 4°C on a rotary shaker, the lysates were centrifuged in an Optima XPN-80 ultracentrifuge (Beckman Coulter, Indiana, USA) at 200,000×g for 90 min and filtered supernatants were loaded on immunoaffinity columns. After a minimum of three passages, columns were washed sequentially with a series of wash buffers[16] and MHC/peptide complexes were eluted with 0.2 N acetic acid. MHC molecules were denatured and the peptides were isolated by adding glacial acetic acid (up to 10%) and heated (76°C). The mixture of peptides, heavy chain and β–2 microglobulin were subjected to reverse-phase high-performance liquid chromatography (RP-HPLC).

Fractionation of the MHC/peptide mixture by RP-HPLC

RP-HPLC was used to reduce the complexity of the peptide mixture eluted from the affinity columns. First, the eluate was dried under vacuum using a CentriVap concentrator (Labconco, Kansas City, Missouri, USA). The solid residue was dissolved in 10% acetic acid and fractionated using a Paradigm MG4 instrument (Michrom BioResources, Auburn, California, USA). An acetonitrile (ACN) gradient was run at pH 2 using a two-solvent system. Solvent A contained 2% ACN in water, and solvent B contained 5% water in ACN. Both solvent A and Solvent B contained 0.1% trifluoroacetic acid. The column was pre-equilibrated at 2% solvent B. Then the sample was loaded at a flow rate of 120 µl/min and a two-segment gradient was run at 160 µl/min flow rate. Fractions were collected in 2 min intervals using a Gilson FC 203B fraction collector (Gilson, Middleton, Wisconsin, USA), and the ultraviolet absorption profile of the eluate was recorded at 215 nm wavelength.[17]

Nano LC-MS/MS analysis

Peptide-containing HPLC fractions were dried and resuspended in a solvent composed of 10% acetic acid and iRT peptides (Biognosys, Schlieren, Switzerland) as internal standards. Fractions were applied individually to an Eksigent nanoLC 415 nanoscale RP-HPLC (AB Sciex, Framingham, Massachusetts, USA), including a 5 mm long, 350 µm internal diameter Chrom XP C18 trap column with 3 µm particles and 120 Å pores, and a 15-cm-long ChromXP C18 separation column (75 µm internal diameter) packed with the same medium (AB Sciex). An ACN gradient was run at pH 2.5 using a two-solvent system. Solvent A was 0.1% formic acid in water, and solvent B was 0.1% formic acid in 95% ACN in water. The column was pre-equilibrated at 2% solvent B. Samples were loaded at 5 µL/min flow rate onto the trap column and run through the separation column at 300 nL/min with two linear gradients: 10% to 40% B for 70 min, followed by 40% to 80% B for 7 min.

The column effluent was ionized using the nanospray III ion source of an AB Sciex TripleTOF 5600 quadruple time-of-flight mass spectrometer (AB Sciex) with the source voltage set to 2400 V. Information-dependent analysis method was used for data acquisition as described in detail by Carreno *et al*.[18] PeakView software V.1.2.0.3 (AB Sciex) was used for data visualization.

Peptide analysis

Peptide sequences were obtained from fragment spectra using PEAKS Studio V.10.5 software (Bioinformatics Solutions, Waterloo, Canada). A database composed of SwissProt Mus musculus (taxon identifier 10090) and iRT peptide sequences was used as the reference for database search. Variable post-translational modifications (PTM) including acetylation, deamination, pyroglutamate formation, oxidation, sodium adducts, phosphorylation, and cysteinylation were included in database search. Identified peptides were further filtered at a false discovery rate of 1% using PEAKS decoy-fusion algorithm.

Immunoablative therapy and splenocyte isolation

Wild-type C57BL/6 mice were purchased from Jackson Laboratories and experiments were performed at the Oklahoma Medical Research Foundation with Institutional Animal Care and Use Committee (IACUC) approval (approval No. 20–28). B16-F10 tumor cells were isolated and washed three times in 1× HBSS. Mice of 6–8 weeks old were inoculated on the right flank with 1×10^5 B16-F10 tumor cells resuspended in 1× HBSS. Once the tumor volume reached 0.5 cm^3, the tumors were either left untreated, injected with 100 µl of 1% GC (Immunophotonics, St. Louis, Missouri, USA), treated with PTT with an 805 nm laser for 10 min at a power density of 0.5W/cm^2, or treated with LIT (combining PTT and GC). Following treatments, the animals were either used for immune analysis or monitored for survival for 100 days or until the animals reached the ethical end points (when the tumor size reached 2.5 cm^3). Eight days post treatment, spleens were isolated and enzymatically digested in serum-free RPMI containing 100 µg/mL Collagenase IV and 20 µg/mL DNase I for 20 min at 37°C. After digestion cells were washed in 1× HBSS, 5% fetal calf serum (FCS), and 5 mM EDTA and then resuspended in RPMI containing 10% FCS and penicillin/streptomycin. For LIT-treated animals that remained tumor-free for >60 days after treatment, they were rechallenged with 1×10^5 B16-F10 tumor cells on the opposite flank. Animals were monitored for tumor growth for 60 days. Animals that grew tumors, spleens were harvested once the tumors reached ~1.8–2 cm^3 and used for enzyme-linked immune absorbent spot (ELISpot). For the animals that remained tumor-free, the spleens were isolated 60 days after rechallenge and used for ELISpot. Log-rank (Mantel-Cox) test was used for statistical analysis of the survival data.

ELISpot

IP, Opaque Plates, sterile 0.45 µm hydrophobic high protein binding immobilon-P membrane plates (Cat# MSIPS4W10) were purchased from MilliporeSigma. Plates were coated overnight with IFN-γ capture antibodies (cat# 16-7313-85) purchased from Invitrogen. Plates were then washed with RPMI and blocked for 2 hours at 37°C with RPMI containing 20% FCS. The 5×10^5 splenocytes were plated and incubated for 36 hours with ~1 µM of tumor peptide purchased from Thermo Fisher Scientific. Plates were washed with 1× PBS containing 0.05% Tween 20 and then incubated with the biotinylated IFN-γ detection antibody (cat#13-7312-85) purchased from Invitrogen, at room temperature for 1 hour, gently shaking. Plates were washed again and incubated with 100 µl of AEC solution for 12–15 min and then washed with water to stop the reaction. Plates were allowed to dry for 24 hours in the dark prior to imaging on the ImmunoSpot ELISpot CTL reader. Spots were counted by the ImmunoSpot analyzer using the default settings on the smart count function. Peptide reactivity was analyzed in duplicate and the average number of spots was calculated. The average number of spots observed in the DMSO negative control was then subtracted from the average number of spots in the well containing peptides to correct for background spots. Number of spots was graphed into GraphPad Prism and one-way ANOVA was used for statistical analysis. P values = *0.5, **0.05, **0.005, ****0.0005.

RESULTS

Localized immuno-ablative therapy effectively eliminates B16-F10 tumors and confers long-term immunity

B16-F10 tumors are highly metastatic, characterized by low immune cell infiltration, and rapid growth.[19 20] To determine if LIT could effectively treat this model, tumor cells were implanted in the flank of mice subcutaneously and allowed to reach a size of 0.5 cm^3 prior to treatment. Following treatments, the animals were either used for immune analysis or monitored for survival for 60–100 days or until the animals reached ethical end points, when tumor reached a size of 2.5 cm (figure 1A). We compared four groups: Untreated (CTRL), GC alone, PTT alone, and LIT (PTT+GC). The animals in CTRL and GC alone groups succumbed to continuous tumor growth within 30 days of tumor inoculation (figure 1B). PTT alone only extended survival of the animals compared with GC and CTRL groups, with 50% of animals surviving 30 days, and only ~15% of animals surviving more than 100 days. However, LIT significantly improved animal survival, with 100% of the animals surviving 30 days, and 50% of the animals surviving tumor-free over 100 days following treatment (figure 1B). This suggests that GC and PTT synergized to achieve antitumor activity (figure 1B). To confirm that LIT generates long-term immunity, LIT-cured animals were rechallenged with B16-F10 tumor cells on the opposite flank once the animals had been tumor-free for >60 days after the initial LIT treatment. We found that about 50% of the LIT-cured animals did not regrow tumors (figure 1C). This demonstrates that LIT successfully generates effective long-term antitumor immunity.

We next investigated the effect of LIT on T cells. The spleens of mice in CTRL, GC, PTT, and LIT groups were isolated 3 and 7 days after treatment following the gating strategy shown in online supplemental figure 1A. The MFI of surface molecules CD28, CD25, and CD69 were evaluated on both $CD4^+$ and $CD8^+$ T cells isolated from the spleen. While there were no significant changes in cellularity of total $CD8^+$ T cells or naïve, memory, and effector $CD8^+$ T cell subtypes, there was significant upregulation of CD28, CD25, and CD69 on $CD8^+CD44^+$, and $CD8^+CD44^{High}CD62L^+$ T cells 72 hours after PTT and LIT (figure 1D, online supplemental figure S1B). A similar upregulation was not observed in $CD4^+$ T-cell subtypes (data not shown). Seven days after treatment the MFI of CD69 was significantly increased in naïve $CD4^+CD62L^+$ T cells and trending up in $CD8^+CD62L^+$ T cells (figure 1E) in both PTT-treated and LIT-treated animals. While CD28 was not increased in either $CD4^+CD62L^+$ or $CD8^+CD62L^+$ T cells, the MFI of CD25 was significantly elevated in $CD8^+CD62L^+$ T cells 7 days after LIT (online supplemental figure S1C). The activation of T cells indicates that PTT is releasing DAMPs and tumor antigens for T-cell targeting. However, the activation of the T cells by PTT alone does not reach the levels of LIT (GC+PTT), suggesting that GC, the immune stimulating component of LIT, is synergizing with PTT to enhance T-cell activation and tumor killing. These observations (figure 1D,E, online supplemental figure S1B,C) correlate with the significant increase in animal survival and prevention of tumor growth on rechallenge (figure 1B,C).

To determine if GC directly activates T cells, total $CD4^+$ and $CD8^+$ T cells were purified from the spleens and co-cultured with GC in vitro. At day 3, T-cell proliferation or CD44 upregulation were not observed, suggesting that GC was unable to activate T cells directly (online supplemental figure 1D). These findings suggest that antigen presenting cells (APCs) are required for T-cell activation, following LIT.

Identification of B16-F10 H2-Db-associated and H2-Kb-associated tumor specific antigens

To assess whether LIT is enhancing existing tumor specific $CD8^+$ T-cell responses or activating de novo $CD8^+$ T-cell responses, we sought to identify tumor-specific antigens (TSAs) expressed by B16-F10 tumor cells in vivo. Murine MHC molecules (H2-Db and H2-Kb) were extracted from tumors as described in methods. Affinity purification columns were set up in series so that both H2-Db and H2-Kb peptidomes were isolated and purified from each tumor (figure 2A). In contrast to B16-F10 tumor cells cultured in vitro which express little-to-no H2-Db or H2-Kb molecules unless treated with IFN-γ (online supplemental figure 2A,B), implanted tumor cells yielded high quantities of MHC class I molecules in vivo. This high

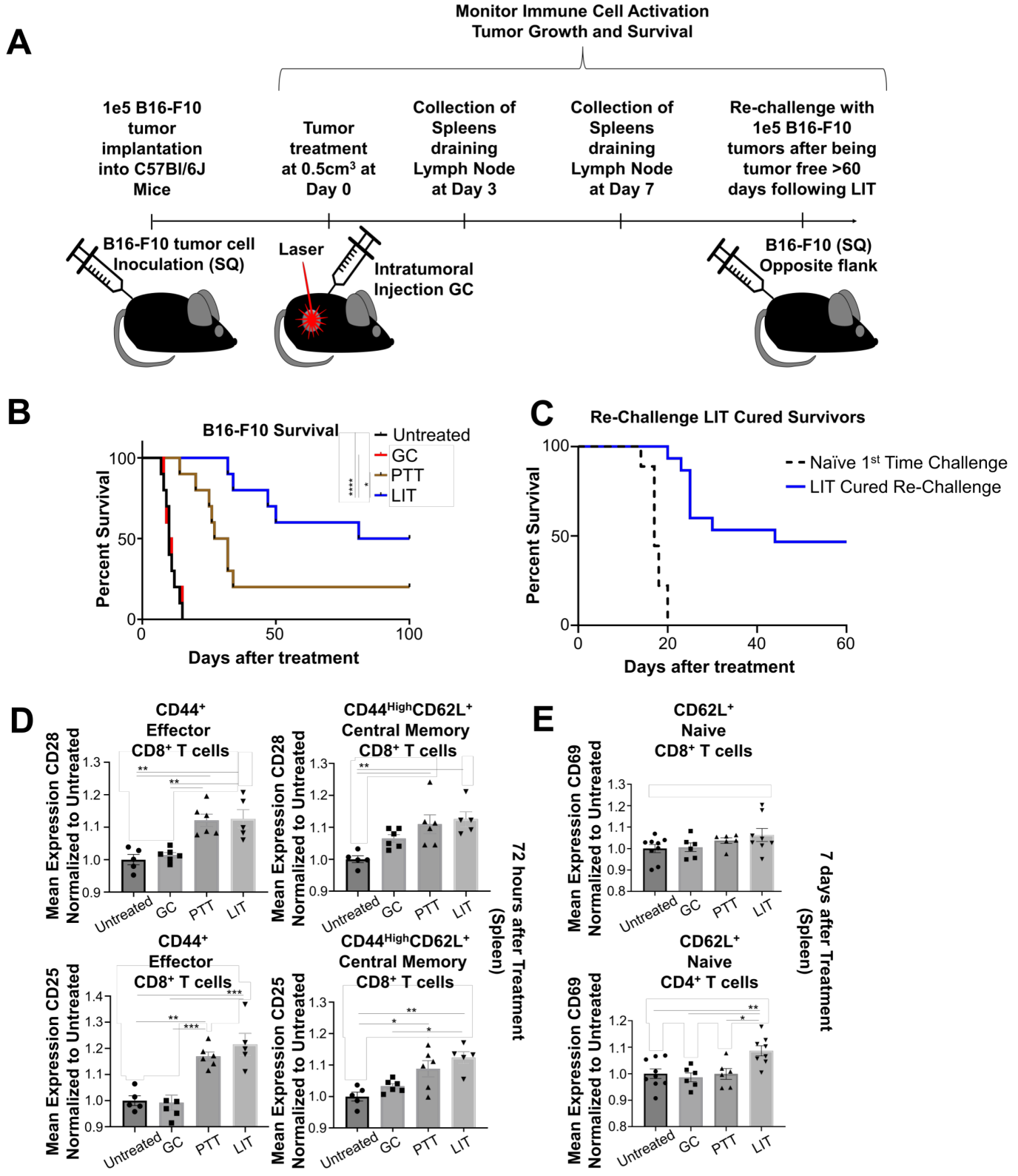

Figure 1 Laser immunotherapy (LIT) cures B16-F10 tumors and confers long-term memory. (A) Schematic of tumor inoculation, LIT treatment, tissue collection, and tumor rechallenge. (B) Survival of animals inoculated with B16-F10 tumors in different treatment groups (untreated, GC alone, PTT alone, or LIT). (C) Survival of LIT-cured animals rechallenged on the opposite flank, compared with untreated first-time challenged controls. Log-rank (Mantel-Cox) test was used for statistical analysis of the survival data. (D) Flow cytometry analysis of the normalized mean expression of CD28 and CD25 on the surface of $CD8^+$ effector and memory T cells from the spleens of animals in different groups 72 hours after treatment. (E) Flow cytometry analysis of the normalized mean expression of CD69 on the surface of naïve CD4 and CD8 naïve T cells from the spleen of animals 7 days after different treatments. One-way analysis of variance was used for statistical analysis of the mean expression data. P values = *0.5, **0.05, **0.005, ****0.0005. GC, N-dihydrogalactochitosan; PTT, photothermal therapy; SQ, subcutaneous.

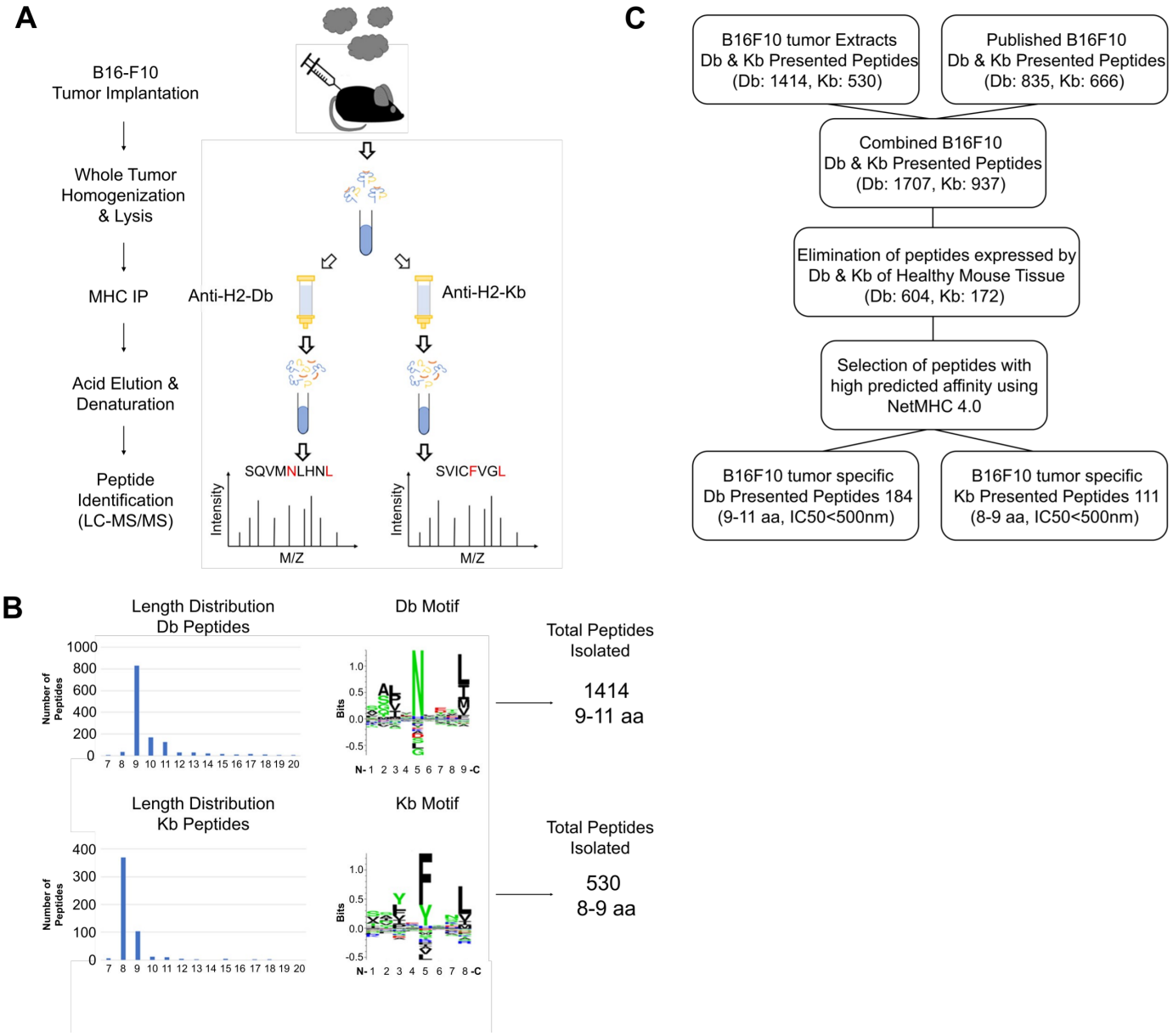

Figure 2 Isolation and characterization of B16-F10 MHC-I peptides. (A) Schematic of the processes of generating tumor extracts, and isolation and identification of H2-Db and H2-Kb peptides. (B) The length distribution, the common motifs, and the total number of non-redundant peptides identified from either the H2-Db or H2-Kb MHC-I allele. (C) Schematic for selection of the tumor-specific peptides to be screened for T-cell reactivity by ELISpot. LC-MS, liquid chromatography coupled mass spectrometry; MHC, major histocompatibility complex.

expression resulted in the identification of hundreds of H2-Db and H2-Kb tumor-associated peptides.

Using liquid chromatography coupled mass spectrometry (LC-MS), we identified a total of 1705 and 628 non-redundant (7–14 aa) H2-Db and H2-Kb peptides, respectively, from which 1414 H2-Db peptides were 9–11 amino acids, and 530 H2-Kb peptides were preferentially 8–9 amino acids (figure 2B and online supplemental tables 1–4).

To generate the most comprehensive B16-F10 tumor-specific peptide library, the B16-F10 H2-Db and H2-Kb peptide repertoires were expanded by adding previously published peptides (835 H2-Db and 666 H2-Kb).[18] When we combined our tumor-specific peptides with the publicly available B16-F10 peptides, the number of non-redundant H2-Db and H2-Kb presented peptides in B16-F10 tumors rose to 1707 and 937, respectively (figure 2C). To identify the TSAs that were exclusively presented by B16-F10 tumor cells and were absent from healthy tissues, the tumor peptidome was searched against a map of murine MHC class I immunopeptidome generated from different tissues of healthy C57BL/6 mice[18] and the peptides expressed on healthy tissues were eliminated. This reduced the number of H2-Db peptides to 604 and H2-Kb peptides to 172 peptides.

To only count for high affinity B16-F10 tumor-specific peptides the list was further narrowed down using the binding affinity criteria of IC50<500 nM (NetMHC 4.0).

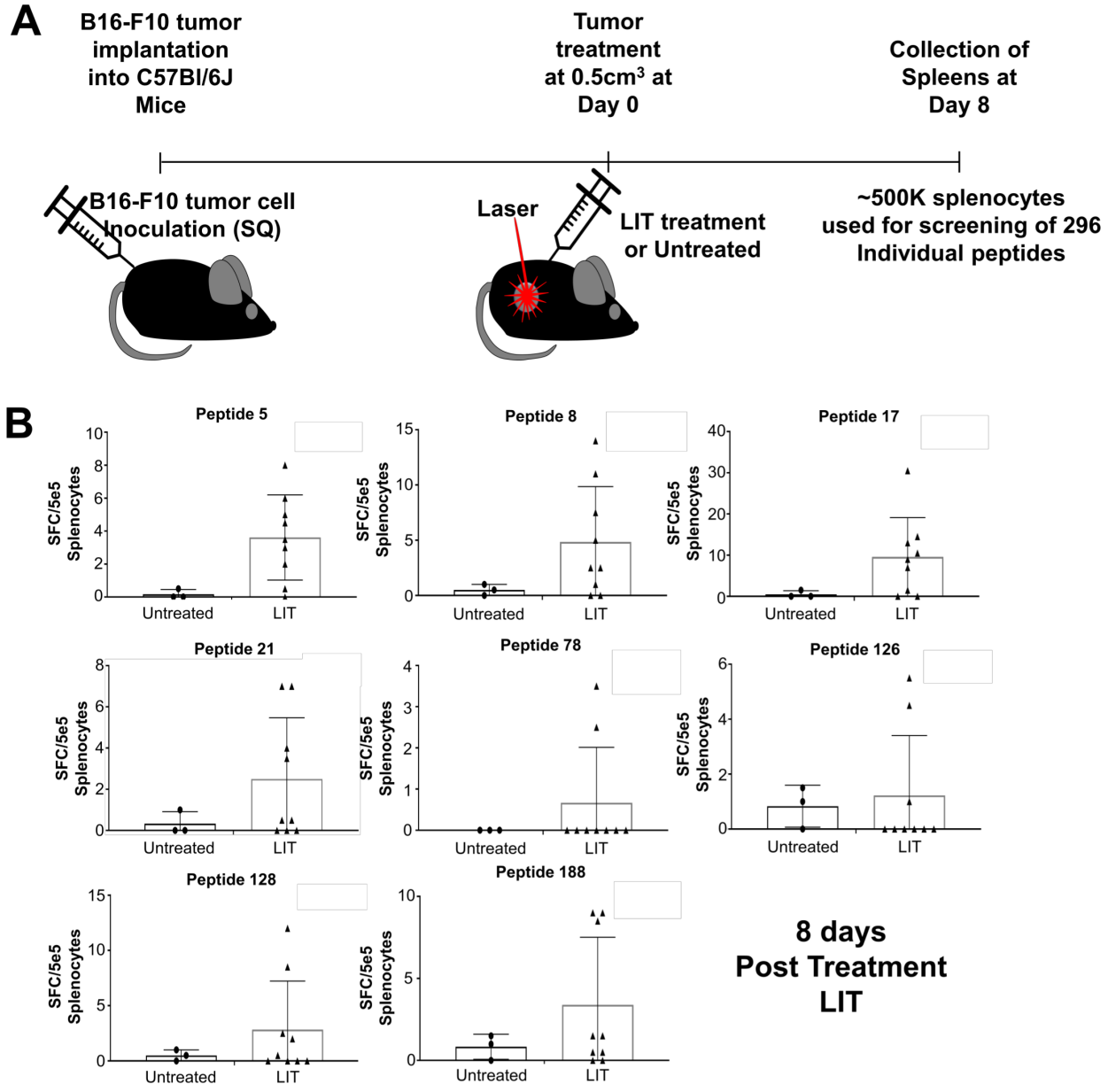

Figure 3 ELISpot screening to identify T cells that recognize tumor-specific peptides in untreated and LIT-treated B16-F10 tumor-bearing animals. (A) Schematic of performing ELISpot for peptide screening. C57BL/6 male and female mice of 6–8 weeks old were injected with 1e5 B16-F10 tumor cells. Once the tumors reached 0.5 cm^3, the tumors were treated with LIT or left untreated. Eight days after treatment splenocytes were isolated and used for ELISpot. (B) Approximately 5e5 total splenocytes were used for the ELISpot with eight selected peptides (~1 µM for each peptide). ELISpots were incubated for ~36 hours prior to developing the ELISpot. Spots were counted using the default settings on the ELISpot reader. Assays were performed in duplicate. The average number of spots in the negative control was then subtracted from the average number of spots in the peptide incubated wells to get the final spot count. LIT, laser immunotherapy; SQ, subcutaneous.

The final list of high-confidence B16-F10 tumor-specific targets comprised of 184 H2-Db and 111 H2-Kb peptides that were selected for T-cell reactivity screening using ELISpot.

We also compared the newly identified B16-F10 peptides and the peptides previously identified in B16-F10 as well as other C57BL/6 tumor-derived cell lines, including EL4 (lymphoma), GL261 (malignant glioma) and LLC1 (Lewis lung carcinoma). Peptide sequence, length, and accession of both unique and shared peptides among different tumor cells have been indicated in online supplemental tables 3 and 4.

Identifying $CD8^+$ T-cell responses to B16-F10 tumor-specific peptides

The 295 peptides specifically expressed on B16-F10 tumor cells (figure 2) were tested for T-cell activity using ELISpot, by determining the frequency of IFN-γ secreting $CD8^+$ T cells that recognize the MHC class I tumor-specific peptides in untreated tumor-bearing and

Table 1 Tumor-specific peptides that generate T-cell reactivity on laser immunotherapy

Peptide ID	Sequence	Length	Source protein	Origin	Allele	IC_{50}
4	AAYAYSAL*	8	Q9CQ22|LTOR1_MOUSE	B16-F10	H2-Kb	4
5	VNYSFRVM†	8	Q810U4|NRCAM_MOUSE	B16-F10	H2-Kb	5.3
6	ASYVYLSM*	8	P09528|FRIH_MOUSE:Q9D5H4|FTMT_MOUSE	B16-F10	H2-Kb	5.4
8	SSFLFWRM†‡	8	P97783|AF1Q_MOUSE	B16-F10	H2-Kb	7
11	IAFKHLFL†	8	Q8R4F0|MCLN3_MOUSE	B16-F10	H2-Kb	8.3
17	VAYCFITI*	8	Q8BWQ6|CP062_MOUSE	B16-F10	H2-Kb	10.9
21	SVICFVGL*	8	P47774|CCR7_MOUSE	B16-F10	H2-Kb	16.3
78	ACPEYSRL*	8	B9EKI3|TMF1_MOUSE	B16-F10	H2-Kb	483.6
82	ANFSFRNTL*†	9	P11344|TYRO_MOUSE	B16-F10	H2-Kb	9.3
85	ANFPRATGL§	9	P0CG14|CTF8A_MOUSE	B16-F10	H2-Kb	31.6
126	FMMWNNHYI†	9	Q8C1B2|PARPT_MOUSE	B16-F10	H2-Db	12.1
128	AQMQNPDTL*	9	Q8R317-2|UBQL1_MOUSE	B16-F10	H2-Db	14.2
183	RVPINETFI*	9	Q8C2E7|WASC5_MOUSE	B16-F10	H2-Db	87.4
188	NTVLNTCTI*	9	Q6DFV6|FN3C1_MOUSE	B16-F10	H2-Db	102.8

*Identified in this study.
†Previously published peptide.[17]
‡Also identified in GL261 tumor cells.[17]
§Also identified in EL4 tumor cells.[17]

LIT-treated animals. Tumors were treated with LIT once they reached 0.5 cm^3. Eight days post treatment splenocytes were isolated and 5×10^5 total splenocytes were used for ELISpot (figure 3A and online supplemental figure S3A,B). Of the 260 peptides screened, 14 had T-cell reactivity in the LIT-treated animals (figure 3B and online supplemental figure S3C). Table 1 provides a detailed information about the peptides that generate T-cell reactivity. Approximately 20–50% of the animals developed $CD8^+$ T-cell reactivity to these peptides during this window following LIT treatment (figure 3B and online supplemental figure S3C). $CD8^+$ T cells in untreated tumor bearing animals did not respond to any of the 14 peptides. These results, which correlate with the extended survival of the LIT-treated animals (figure 1B), suggest that eliciting the $CD8^+$ T-cell response to these 14 tumor-specific peptides could be one of the mechanisms behind the improved survival of animals following LIT and warrant further investigation.

Animals cured by immuno-ablative therapy have increased numbers of tumor-specific $CD8^+$ T cells on tumor rechallenge

To determine if the peptide-specific $CD8^+$ T cells, shown in figure 3B and online supplemental figure S3C, are also involved in long-term antitumor immunity, LIT-cured animals were rechallenged on the opposite flank with B16-F10 tumors (figure 4A). Some of the LIT-cured mice developed tumors on rechallenge and we isolated the spleens of these animals for ELISpot once the tumors reached ethical endpoints. For animals that remained tumor-free, the spleens were isolated 60 days after rechallenge for ELISpot (online supplemental figure S4). Of the 14 peptides highlighted in figure 3B and online supplemental figure S3C, all five tumor-free animals had reactivity to peptides 17 and 188 (figure 4B). Four animals showed reactivity to peptides 5, 8, 21, 78, 82, and 126 (figure 4B and online supplemental figure S4B) and three displayed reactivity to peptides 6, 11, and 128 (online supplemental figure 4B). Interestingly, the LIT-cured animals that failed to resist tumor rechallenge had very little reactivity to these peptides (figure 4B and online supplemental figure 4B). These data indicate that $CD8^+$ T-cell responses to these tumor-specific peptides provide antitumor immunity and play an important role in tumor rejection. Furthermore, these data support the notion that LIT generates de novo $CD8^+$ T-cell responses that can effectively eliminate these tumors and confer long-term protection on tumor rechallenge.

DISCUSSION

Our previous works have demonstrated that LIT can effectively treat a variety of tumors in different animal models and cancer patients.[21–23] However, the mechanism of LIT is not fully understood. Here, we demonstrate that LIT generated de novo T-cell responses to immunologically 'cold' tumors, in addition to enhancing the existing antitumor immune response. Results in figure 1 shows that LIT greatly enhances the survival of B16-F10 tumor-bearing animals and protects 'cured' animals from tumor rechallenge. Moreover, LIT enhances the activation of T cells found in the tumor draining lymph nodes and the spleen following treatment (figure 1D–E). After characterizing the B16-F10 tumor-specific peptides (figure 2) and screening them for T-cell reactivity (figure 3), we identified six immunogenic peptides (figure 4B). T

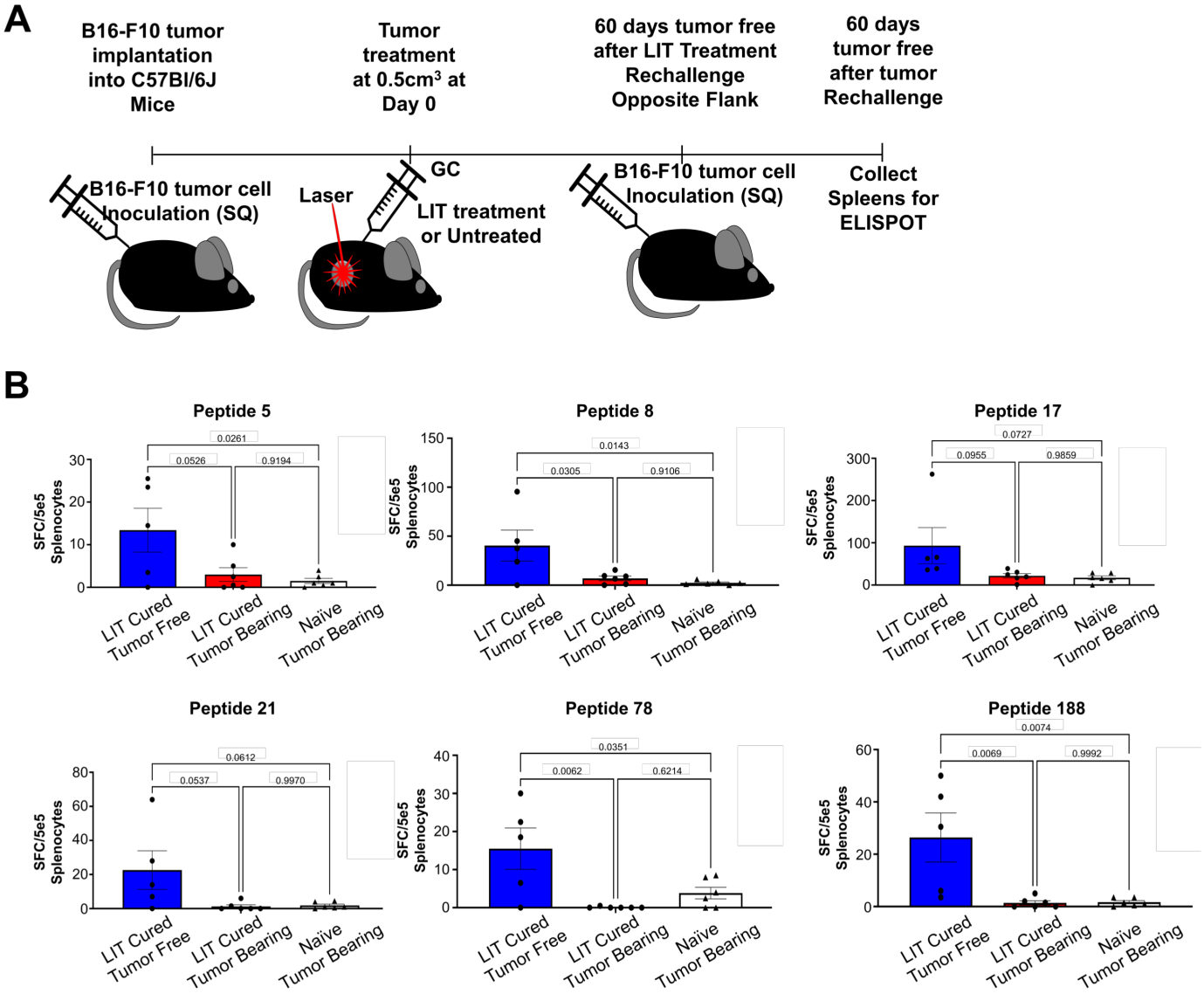

Figure 4 Tumor-specific peptide T-cell reactivity in LIT-cured animals that remained tumor-free following tumor rechallenge. (A) Schematic of processes of LIT treatment, tumor rechallenge, and spleen collection for ELISpot. C57BL/6 mice of 6–8 weeks old were injected with 1e5 B16-F10 tumor cells. Once the tumors reached 0.5 cm^3, they were treated with LIT or left untreated. LIT-cured mice were then rechallenged on the opposite flank after being tumor-free for >60 days. Once the animals were tumor-free for >60 days following tumor rechallenge, splenocytes were isolated and incubated with B16-F10-specific peptides for ~36 hours before being developed. The LIT-cured animals that grew tumors on rechallenge were terminated once tumor volume reached ethical time points and the spleens were isolated for ELISpot. (B) Approximately 5e5 total splenocytes were used for the ELISpot with six selected peptides (~1 µM for each peptide). ELISpots were incubated for ~36 hours prior to developing the ELISpot. Spots were counted using the default settings on the ELISpot reader. Assays were performed in duplicate. The average number of spots in the negative control was then subtracted from the average number of spots in the peptide incubated wells to get the final spot count. The number was graphed, and each dot represents an individual animal. One-way analysis of variance was used for statistical analysis. P values = *0.5, **0.05, **0.005, ****0.0005. ELISpot, enzyme-linked immune absorbent spot; GC, N-dihydrogalactochitosan; LIT, laser immunotherapy; SQ, subcutaneous

cells in untreated tumor-bearing animals and LIT-cured animals that failed to resist tumor rechallenge showed little-to-no reactivity to these six peptides (figure 4B). However, in LIT-cured animals that remained tumor-free on tumor rechallenge, there were significantly elevated $CD8^+$ T-cell responses to these peptides, suggesting de novo $CD8^+$ T-cell responses. On the other hand, it is possible that our observed de nova generation of T-cell responses could be the expansion of a low numbers of existing antigen-specific T cells induced by LIT treatment. Future studies, expanding TILs or splenocytes before ELISpot will shed light on this question.

As demonstrated in this study, PTT plays an important role in LIT. Consistent with the immunological effects of PTT observed in our work, others have demonstrated that the melanin in the B16-F10 tumors allows for significant heat absorption which stimulates antitumor immune responses. Moreover, it has been shown that melanin

from the B16-F10 tumors can activate T-cell responses capable of delaying tumor growth.[24] Furthermore, we have observed the activation of central-memory (Tcm), and effector-memory (Tem) T cells, and tissue-resident memory $CD8^+$ T cells by LIT in this study, consistent with the previous observations.[25] However, in our work and others, increased heat absorption and melanin-stimulated immune responses are not sustainable, and the tumor usually continues to grow after a period. It is the combination of thermal ablation and with GC that the immune response is sustained, and the animals become tumor-free with some of them resistant to tumor rechallenge. Based on our current study, it is unclear how melanin-initiated antitumor immune response and PTT alone contribute to the development of LIT-induced antitumor immunity. Future work will focus on their contributions.

Reprograming the immune system to recognize and kill cancer cells holds unlimited potential. It provides constant immune surveillance and tumor destruction to eliminate metastatic niches and to prevent tumor recurrance.[26–28] The concept of harnessing the body's immune system to fight cancer from within has led to different immunotherapeutic approaches.[28–31] This has led to a paradigm shift in generating novel treatment approaches to treating various tumors. The most widely used immunotherapies are immune checkpoint therapies (ICTs) that specifically target the T cell inhibiting ligands PD-1 (programmed cell death protein-1) and CTLA-4 (cytotoxic T-lymphocytes-associated protein 4), and the PD-1 ligand PD-L1. CTLA-4 and PD-1 are present on the surface of T cells while PD-L1 is expressed on the surface of tumor cells and APCs.[32–34] Blocking either of these molecules has achieved enhanced T-cell mediated tumor killing and tumor regression. While these therapies hold great promise theoretically, the patient response rate across a broad range of cancers depending on the tumor type is generally <30, well below an acceptable rate.[35]

Based on our preliminary studies we hypothesize that immune-ablative therapies would be increasing the effectiveness of ICT. Currently, patients are grouped into three categories according to their responses to ICT: primary resistance, adaptive resistance, and acquired resistance.[36–39] Primary resisters fail to respond to ICT due to either insufficient T-cell responses, low tumor mutational burden, low/lack of tumor peptide presentation, and/or an unfavorable TME. In this study, we have demonstrated that LIT results in generation of novel neoantigens that can potentially overcome an unfavorable TME of a poorly immunogenic 'cold' tumor and produce sufficient antitumor T-cell responses to prevent tumor growth on tumor rechallenge. Therefore, combination-based LIT approaches could modulate the TME and dramatically increase the efficacy of ICT in these primary resistance patients.

Adaptive immune resisters have existing, sufficient T-cell responses, but the TIME actively prevents tumor killing. In this scenario, we posit that LIT can enhance the existing T-cell response by reprogramming the established TIME, releasing DAMPs and tumor antigens to recruit and stimulate antitumor T cells, while generating a proinflammatory TME via the addition of an immune stimulant. Acquired resisters, which initially respond to ICT but eventually relapse, also lack a sustained tumor-specific T-cell response. Adaptive resistance and acquired resistance patients would both benefit from LIT through remodeling of the suppressive TME and generation of de novo T-cell responses.

In summary, the LIT generated de novo T-cell responses hold great potential for the treatment of immunological 'cold', metastatic tumors. Furthermore, it can potentially be used to synergize with other immunotherapies, such as ICT, that depends on sufficient T-cell population and/or T-cell responses. We will test these concepts by using LIT to overcome ICT resistance, to enhance the efficacy of current immunotherapies for future clinical applications.

Author affiliations
[1]Stephenson School of Biomedical Engineering, The University of Oklahoma, Norman, Oklahoma, USA
[2]Department of Microbiology and Immunology, The University of Oklahoma Health Sciences Center, Oklahoma City, Oklahoma, USA
[3]Arthritis & Clinical Immunology Research Program, Oklahoma Medical Research Foundation, Oklahoma City, Oklahoma, USA
[4]Medical Oncology/TSET Phase 1 Program, The University of Oklahoma Stephenson Cancer Center, Oklahoma City, Oklahoma, USA
[5]Institute for Immunity, Stanford University School of Medicine, Stanford, California, USA
[6]Departments of Molecular and Cellular Physiology and Structural Biology, Stanford University School of Medicine, Stanford, California, USA
[7]Department of Microbiology and Immunology, Stanford University School of Medicine, Stanford, California, USA

Contributors Conceptualization: ARH, SK, WHH, and WRC. Methodology and Experiments: ARH, SK, and JRK. Visualization: ARH and SK. Funding acquisition: WRC. Project administration: WRC. Supervision: WHH and WRC. Writing—original draft: ARH, SK, and WRC. Writing—review and editing: X-HS, ARN, QY, XY, KCG, and MMD. Guarantor of the overall content: WRC.

Funding This work was supported in part by the National Cancer Institute (R01CA205348) and the Oklahoma Center for the Advancement of Science and Technology (HR16-085 and HF20-019). It was also supported in part by the National Cancer Institute Cancer Center Support Grant P30CA225520 awarded to the University of Oklahoma Stephenson Cancer Center and used the Molecular Biology and Cytometry Research Shared Resource.

Competing interests WRC is co-founder and an unpaid member of the Board of Directors of Immunophotonics. Other authors confirm that there is no known conflict of interest associated with this publication. There was no financial support that influenced the conclusions of this manuscript. This work has not been published by other journals and is not concurrently being considered for publication by another journal. All authors have read and approved the manuscript.

Patient consent for publication Not applicable.

Ethics approval Not applicable.

Provenance and peer review Not commissioned; externally peer reviewed.

Data availability statement Data are available upon reasonable request. The raw data supporting the conclusions of this article will be made available by the authors, without undue reservation. The H2-Db and H2-Kb presented peptides from B16-F10 tumors identified in the study are available in Supplementary Tables 1 and 2.

of the translations (including but not limited to local regulations, clinical guidelines, terminology, drug names and drug dosages), and is not responsible for any error and/or omissions arising from translation and adaptation or otherwise.

ORCID iDs
Ashley R Hoover http://orcid.org/0000-0002-3555-1510
Saghar Kaabinejadian http://orcid.org/0000-0002-8434-8703
Jason R Krawic http://orcid.org/0000-0003-0103-0212
Wei R Chen http://orcid.org/0000-0002-7133-5794

REFERENCES

1 Ward JP, Gubin MM, Schreiber RD. Chapter Two - The Role of Neoantigens in Naturally Occurring and Therapeutically Induced Immune Responses to Cancer. In: Schreiber RD, ed. *Advances in immunology*. Academic Press, 2016: 25–74.
2 Morrison BJ, Steel JC, Morris JC. Reduction of MHC-I expression limits T-lymphocyte-mediated killing of Cancer-initiating cells. *BMC Cancer* 2018;18:469.
3 Dhatchinamoorthy K, Colbert JD, Rock KL. Cancer immune evasion through loss of MHC class I antigen presentation. *Front Immunol* 2021;12:636568.
4 Cornel AM, Mimpen IL, Nierkens S. MHC class I downregulation in cancer: underlying mechanisms and potential targets for cancer immunotherapy. *Cancers* 20201760;12. [Epub ahead of print: 02 07 2020]. doi:10.3390/cancers12071760
5 Paluskievicz CM, Cao X, Abdi R, *et al*. T regulatory cells and priming the suppressive tumor microenvironment. *Front Immunol* 2019;10:2453–53.
6 Facciabene A, Motz GT, Coukos G. T-regulatory cells: key players in tumor immune escape and angiogenesis. *Cancer Res* 2012;72:2162–71.
7 Li K, Shi H, Zhang B, *et al*. Myeloid-derived suppressor cells as immunosuppressive regulators and therapeutic targets in cancer. *Signal Transduct Target Ther* 2021;6:362.
8 Yang Y, Li C, Liu T, *et al*. Myeloid-derived suppressor cells in tumors: from mechanisms to antigen specificity and microenvironmental regulation. *Front Immunol* 2020;11:1371.
9 Liu K, Hoover AR, Krawic JR, *et al*. Antigen presentation and interferon signatures in B cells driven by localized ablative cancer immunotherapy correlate with extended survival. *Theranostics* 2022;12:639–56.
10 Hoover AR, Liu K, DeVette CI, *et al*. Single-cell RNA sequencing reveals localized tumour ablation and intratumoural immunostimulant delivery potentiate T cell mediated tumour killing. *Clin Transl Med* 2022;12:e937.
11 Lu C, Klement JD, Ibrahim ML, *et al*. Type I interferon suppresses tumor growth through activating the STAT3-granzyme B pathway in tumor-infiltrating cytotoxic T lymphocytes. *J Immunother Cancer* 2019;7:157.
12 Fuertes MB, Kacha AK, Kline J, *et al*. Host type I IFN signals are required for antitumor CD8+ T cell responses through CD8{alpha}+ dendritic cells. *J Exp Med* 2011;208:2005–16.
13 Duong E, Fessenden TB, Lutz E, *et al*. Type I interferon activates MHC class I-dressed CD11b^{+} conventional dendritic cells to promote protective anti-tumor CD8^{+} T cell immunity. *Immunity* 2022;55:308–23.
14 Hoover AR, Liu K, DeVette CI. ScRNA-seq reveals tumor microenvironment remodeling induced by local intervention-based immunotherapy. *bioRxiv* 2020:2020;323006:10.02..
15 Wang J, Saffold S, Cao X, *et al*. Eliciting T cell immunity against poorly immunogenic tumors by immunization with dendritic cell-tumor fusion vaccines. *J Immunol* 1998;161:5516–24.
16 Purcell AW, Ramarathinam SH, Ternette N. Mass spectrometry-based identification of MHC-bound peptides for immunopeptidomics. *Nat Protoc* 2019;14:1687–707.
17 Kaabinejadian S, Barra C, Alvarez B, *et al*. Accurate MHC motif deconvolution of Immunopeptidomics data reveals a significant contribution of DRB3, 4 and 5 to the total DR immunopeptidome. *Front Immunol* 2022;13:835454.
18 Carreno BM, Magrini V, Becker-Hapak M, *et al*. Cancer immunotherapy. A dendritic cell vaccine increases the breadth and diversity of melanoma neoantigen-specific T cells. *Science* 2015;348:803–8.
19 Mosely SIS, Prime JE, Sainson RCA, *et al*. Rational selection of syngeneic preclinical tumor models for immunotherapeutic drug discovery. *Cancer Immunol Res* 2017;5:29–41.
20 Tomita M, Yasui H, Higashikawa K, *et al*. Anti PD-1 treatment increases [^{18}F]FDG uptake by cancer cells in a mouse B16F10 melanoma model. *EJNMMI Res* 2018;8:82.
21 Li X, Naylor MF, Le H, *et al*. Clinical effects of in situ photoimmunotherapy on late-stage melanoma patients: a preliminary study. *Cancer Biol Ther* 2010;10:1081–7.
22 Naylor MF, Zhou F, Geister BV, *et al*. Treatment of advanced melanoma with laser immunotherapy and ipilimumab. *J Biophotonics* 2017;10:618–22.
23 Zhou F, Li X, Naylor MF, *et al*. InCVAX--a novel strategy for treatment of late-stage, metastatic cancers through photoimmunotherapy induced tumor-specific immunity. *Cancer Lett* 2015;359:169–77.
24 Ye Y, Wang C, Zhang X, *et al*. A melanin-mediated cancer immunotherapy patch. *Sci Immunol* 2017;2. doi:10.1126/sciimmunol.aan5692. [Epub ahead of print: 10 11 2017].
25 Menares E, Gálvez-Cancino F, Cáceres-Morgado P, *et al*. Tissue-resident memory CD8^{+} T cells amplify anti-tumor immunity by triggering antigen spreading through dendritic cells. *Nat Commun* 2019;10:4401.
26 Papaioannou NE, Beniata OV, Vitsos P, *et al*. Harnessing the immune system to improve cancer therapy. *Ann Transl Med* 2016;4:261–61.
27 Walsh SR, Simovic B, Chen L, *et al*. Endogenous T cells prevent tumor immune escape following adoptive T cell therapy. *J Clin Invest* 2019;129:5400–10.
28 Gong J, Chehrazi-Raffle A, Reddi S, *et al*. Development of PD-1 and PD-L1 inhibitors as a form of cancer immunotherapy: a comprehensive review of registration trials and future considerations. *J Immunother Cancer* 2018;6:8.
29 Yang Y. Cancer immunotherapy: harnessing the immune system to battle cancer. *J Clin Invest* 2015;125:3335–7.
30 Waldman AD, Fritz JM, Lenardo MJ. A guide to cancer immunotherapy: from T cell basic science to clinical practice. *Nat Rev Immunol* 2020;20:651–68.
31 Hegde PS, Chen DS. Top 10 challenges in cancer immunotherapy. *Immunity* 2020;52:17–35.
32 Qin S, Xu L, Yi M, *et al*. Novel immune checkpoint targets: moving beyond PD-1 and CTLA-4. *Mol Cancer* 2019;18:155.
33 Lei Q, Wang D, Sun K, *et al*. Resistance mechanisms of Anti-PD1/PDL1 therapy in solid tumors. *Front Cell Dev Biol* 2020;8:672.
34 De Silva P, Aiello M, Gu-Trantien C, *et al*. Targeting CTLA-4 in cancer: is it the ideal companion for PD-1 blockade immunotherapy combinations? *Int J Cancer* 2021;149:31–41.
35 Haslam A, Prasad V. Estimation of the percentage of US patients with cancer who are eligible for and respond to checkpoint inhibitor immunotherapy drugs. *JAMA Netw Open* 2019;2:e192535–e35.
36 Sharma P, Hu-Lieskovan S, Wargo JA, *et al*. Primary, adaptive, and acquired resistance to cancer immunotherapy. *Cell* 2017;168:707–23.
37 Veldman J, Visser L, Berg Avanden, *et al*. Primary and acquired resistance mechanisms to immune checkpoint inhibition in Hodgkin lymphoma. *Cancer Treat Rev* 2020;82:101931.
38 Oba T, Long MD, Keler T, *et al*. Overcoming primary and acquired resistance to anti-PD-L1 therapy by induction and activation of tumor-residing cDC1s. *Nat Commun* 2020;11:5415.
39 Bai R, Chen N, Li L, *et al*. Mechanisms of cancer resistance to immunotherapy. *Front Oncol* 2020;10.

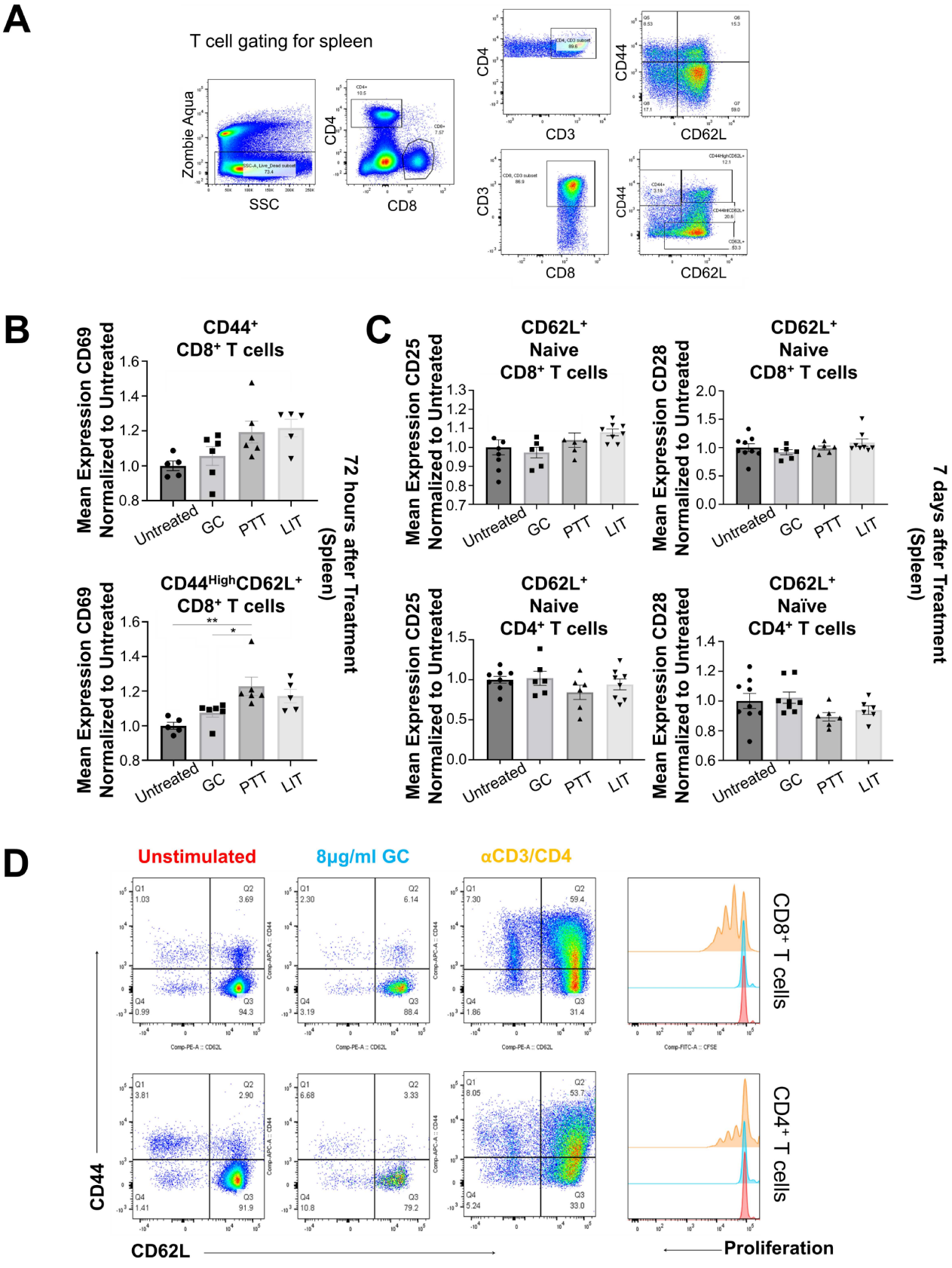
A
T cell gating for spleen
Zombie Aqua
SSC
CD4
CD8
CD3
CD44
CD62L
B
CD44+ CD8+ T cells
CD44HighCD62L+ CD8+ T cells
Mean Expression CD69 Normalized to Untreated
Untreated
GC
PTT
LIT
72 hours after Treatment (Spleen)
C
CD62L+ Naive CD8+ T cells
CD62L+ Naive CD4+ T cells
Mean Expression CD25 Normalized to Untreated
Mean Expression CD28 Normalized to Untreated
7 days after Treatment (Spleen)
D
Unstimulated
8µg/ml GC
αCD3/CD4
CD8+ T cells
CD4+ T cells
CD44
CD62L
Proliferation

Figure S2

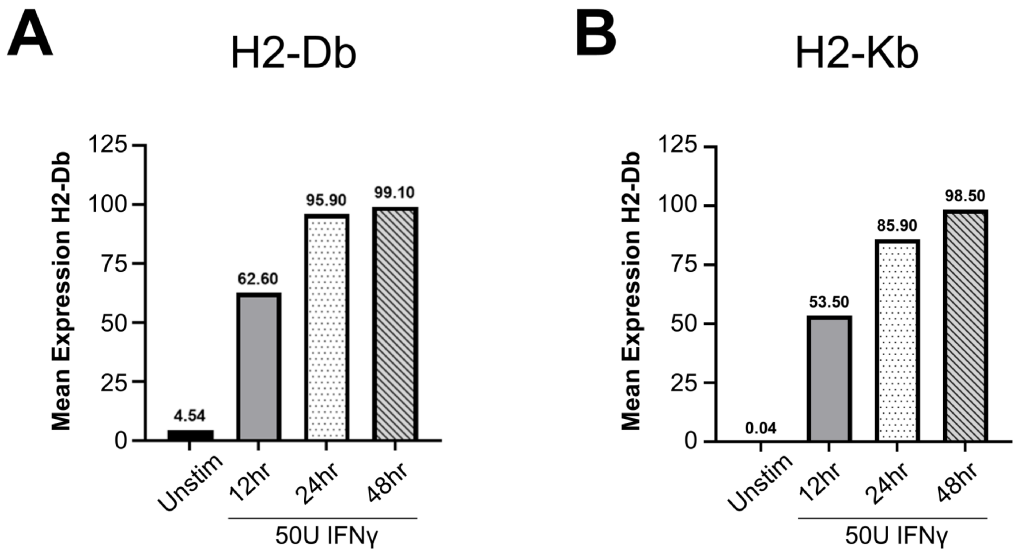
A
H2-Db
Mean Expression H2-Db
125
100
75
50
25
0
4.54
62.60
95.90
99.10
Unstim
12hr
24hr
48hr
50U IFNγ
B
H2-Kb
Mean Expression H2-Db
125
100
75
50
25
0
0.04
53.50
85.90
98.50
Unstim
12hr
24hr
48hr
50U IFNγ

Figure S3

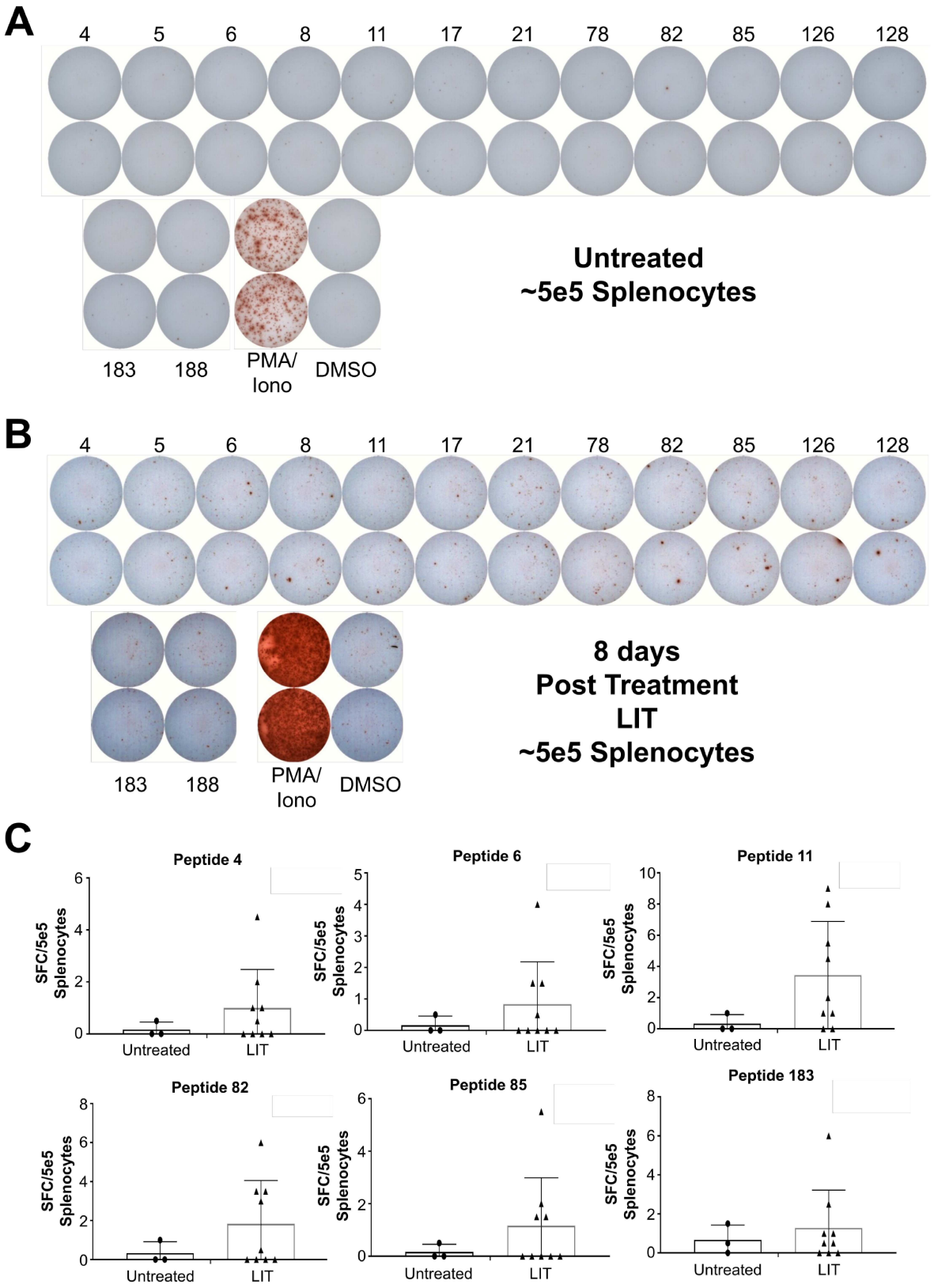
A
4 5 6 8 11 17 21 78 82 85 126 128
183 188 PMA/ Iono DMSO
Untreated
~5e5 Splenocytes
B
4 5 6 8 11 17 21 78 82 85 126 128
183 188 PMA/ Iono DMSO
8 days
Post Treatment
LIT
~5e5 Splenocytes
C
Peptide 4
Peptide 6
Peptide 11
Peptide 82
Peptide 85
Peptide 183
SFC/5e5 Splenocytes
Untreated
LIT

Figure S4

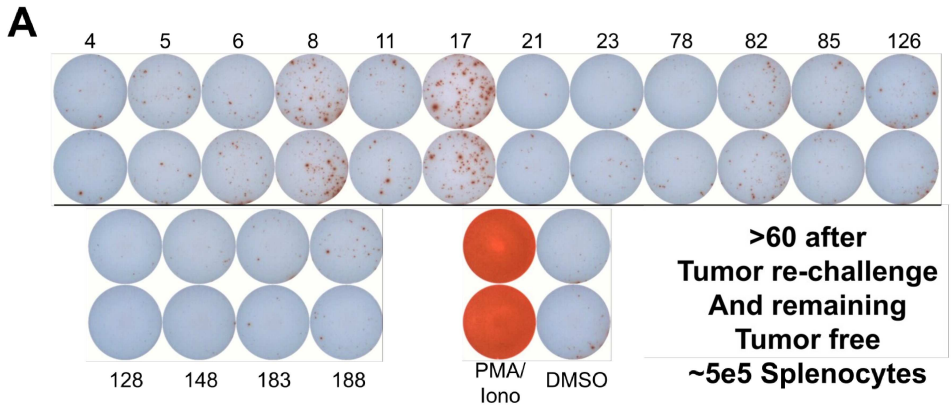
A
4
5
6
8
11
17
21
23
78
82
85
126
128
148
183
188
PMA/
Iono
DMSO
>60 after
Tumor re-challenge
And remaining
Tumor free
~5e5 Splenocytes

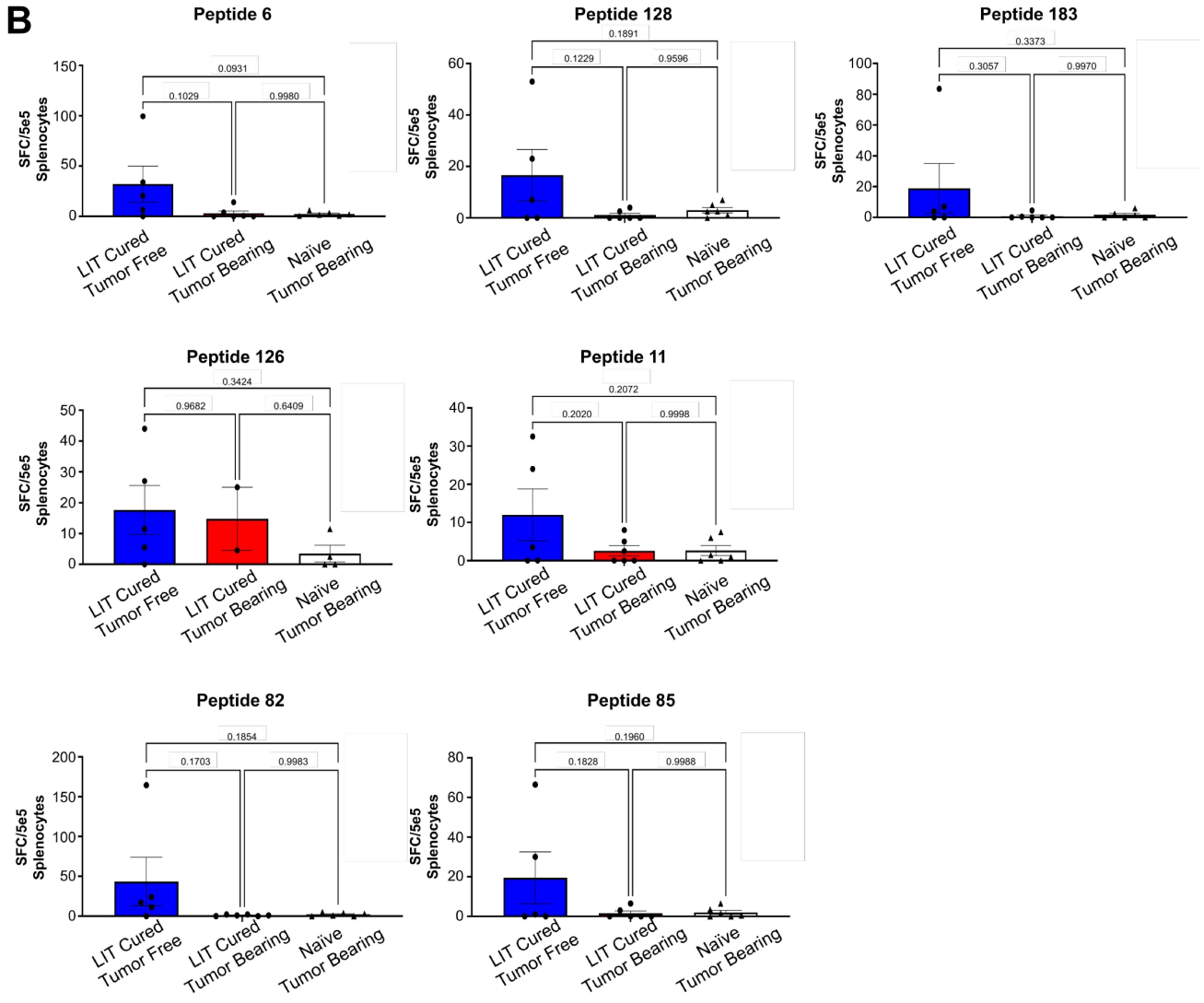
B
Peptide 6
Peptide 128
Peptide 183
Peptide 126
Peptide 11
Peptide 82
Peptide 85
SFC/5e5 Splenocytes
LIT Cured Tumor Free
LIT Cured Tumor Bearing
Naïve Tumor Bearing

Supplemental Figure 1

LIT activation of T cells within the spleen. (A) Flow cytometry gating used for analysis of the $CD4^+$ and $CD8^+$ T cells. (B) Flow cytometry analysis of the normalized mean expression of CD69 on the surface of $CD8^+$ effector and memory T cells from the spleens of animals in different groups 72 hours after treatment. (C) Flow cytometry analysis of the normalized mean expression of CD25 and CD25 on the surface of naïve CD4 and CD8 naïve T cells from the animal spleens seven days after treatment. One-way ANOVA was used for statistical analysis of the mean expression data. P values = *0.5, **0.05, **0.005, ****0.0005. (D) Flow cytometry analysis of CD44, CD62L, and CFSE expression of either purified $CD4^+$ or $CD8^+$ T cells from the spleens. T cells were incubated with either GC or anti-CD3/anti-CD28 for 72 hours prior to flow analysis.

Supplemental Figure 2

In vitro characterization of B16-F10 H2-Db and H2-Kb expression following 50 U/mL of IFNγ stimulation (A-B). Analysis of the expression of (A) H2Db and (B) H2Kb MHC-I molecules on B16-F10 cells grown in vitro. The mean expression of H2-Db or H2-Kb was examined after 12, 24, and 48 hours via flow cytometry. Expression of H2-Db or H2-Kb is represented as a bar graph.

Supplemental Figure 3

ELISpot screening of tumor specific peptides in untreated and LIT B16-F10 tumor-bearing animals. (A-C) C57BL/6 mice of 6-8-week-old were injected with 1e5 B16-F10 tumor cells. Once the tumors reached $0.5cm^3$, the tumors were treated with LIT or left untreated. Eight days after treatment splenocytes were isolated and used for ELISPOT. Approximately 5e5 total splenocytes were used for the ELISPOTs with ~1μM peptide. ELISPOTs were incubated for ~36 hours prior to developing the ELISPOT. Spots were counted using the default settings on the ELISPOT reader. Assays were performed in duplicate. The average number of spots in the negative control was then subtracted from the average number of spots in the peptide incubated wells to get the final spot count. (A) ELISPOT using splenocytes from untreated tumor-bearing animals. (B) ELISPOT using splenocytes from LIT treated animals 8 days after treatment. (C) Spot-forming cells (SFC) per well were calculated using the following formula for six selected peptides, Average spots peptide wells – Average spots DMSO wells = final spot count per well and graphed.

Supplemental Figure 4

Tumor specific peptide T cell reactivity in LIT-cured animals that resisted tumor rechallenge. (A-B) C57BL/6 mice of 6–8-week-old were injected with 1e5 B16-F10 tumor cells. Once the tumors reached $0.5cm^3$, the tumors were treated with LIT or left untreated. LIT-cured survivors were then rechallenged on the opposite flank after being tumor free for >60days. Once the animals were tumor free for >60days following tumor rechallenge, splenocytes were isolated and incubated with B16-F10 specific peptides for ~36 hours before being developed. Approximately 5e5 total splenocytes from LIT-cured tumor rechallenged non-tumor-bearing animals were used to ELISpots with ~1μM peptide. ELISpots were incubated for ~36 hours prior to developing the ELISpot. (A) ELISPOT using splenocytes from LIT-cured animals that resisted tumor rechallenge. (B) Spot-forming cells (SFC) were counted using the default settings on the ELISPOT reader for seven selected peptides. Assays were performed in duplicate. The average number of spots in the negative control was then subtracted from the average number of spots in the peptide incubated wells to get the final spot count. The number was graphed, and each dot represents an individual animal. One-Way ANOVA was used for statistical analysis. P values = *0.5, **0.05, **0.005, ****0.0005.